

Cite this: *RSC Advances*, 2011, 1, 397–400

www.rsc.org/advances

## COMMUNICATION

## Hierarchical nickel sulfide hollow spheres for high performance supercapacitors†

By Ting Zhu, Zhiyu Wang, Shujiang Ding, Jun Song Chen\* and Xiong Wen (David) Lou\*

Received 28th May 2011, Accepted 29th June 2011

DOI: 10.1039/c1ra00240f

Hierarchical NiS hollow spheres assembled from ultrathin nanosheets are synthesized by an efficient template-engaged conversion method. Silica nanospheres were used as templates, and  $\text{SiO}_2$ @nickel silicate core-shell nanostructures were first prepared. In the presence of  $\text{Na}_2\text{S}$ , the nickel silicate shell completely transformed into NiS nanosheets *via* a hydrothermal treatment, accompanied by the total dissolution of the inner  $\text{SiO}_2$  core. This gives rise to uniform hollow nanospheres whose shells are assembled from ultrathin NiS nanosheets. In virtue of the large surface area and enhanced structural stability, the as-prepared NiS hollow spheres exhibit excellent electrochemical performance as electrode materials for supercapacitors.

Hollow micro/nanostructures have attracted tremendous research interest in a myriad of applications, such as lithium-ion batteries,<sup>1–4</sup> catalysis,<sup>5–6</sup> chemical sensors<sup>7–9</sup> and biomedical applications,<sup>10–14</sup> due to their unique structural features including well-defined interior voids, low density, large surface area and surface permeability.<sup>15</sup> Templating against colloidal particles is regarded as the most straightforward and effective route towards hollow structures with narrow size distributions and well-defined shapes.<sup>16–18</sup> In general, templating methods involve the growth of a shell of designed materials on various colloidal templates (*e.g.*, monodisperse latex and silica spheres) and subsequent removal of the template to generate the interiors with desirable complexity. The use of templates in principle allows one to manipulate the size and morphology of resultant hollow particles for better control of the local chemical environment and extraordinary properties. However, difficulties ranging from material incompatibility to the collapse or deformation of hollow structures upon template removal are common in practice. The disadvantage of being time-consuming and the general requirement of a tedious multistep procedure also greatly restrict the extensive application of templating methods.

Nickel sulfides with many different phases such as NiS,  $\text{NiS}_2$ ,  $\beta\text{-Ni}_3\text{S}_2$ ,  $\alpha\text{-Ni}_{3+x}\text{S}_2$ ,  $\text{Ni}_4\text{S}_{3+x}$ ,  $\text{Ni}_6\text{S}_5$ ,  $\text{Ni}_7\text{S}_6$ ,  $\text{Ni}_9\text{S}_8$  and  $\text{Ni}_3\text{S}_4$  are inexpensive and abundant materials with widespread applications as ceramic tougheners, hydrogenation catalysts and electrode materials,

*etc.*<sup>19–23</sup> Despite the success in the synthesis of various morphologies, including nanochains,<sup>24</sup> hollow spheres<sup>25–26</sup> and layer-rolled structures,<sup>27</sup> the preparation of uniform hierarchical hollow structures of nickel sulfides still remains as a significant challenge. Herein, we report an effective conversion route for controllable synthesis of uniform NiS hollow spheres with a hierarchical structure by template-engaged precipitation of nickel silicates and subsequent *in situ* chemical conversion to NiS phase. Remarkably, these formed hollow spheres are entirely assembled from ultrathin NiS nanosheets with a thickness of a few nanometres, and simultaneously the silica cores are completely removed during the conversion reaction in a basic solution. When evaluated for potential use in supercapacitors, the NiS hierarchical hollow spheres exhibit excellent electrochemical performance due to their unique structure and high surface area.

The scheme in Fig. 1 illustrates our concept for the synthesis of NiS hollow spheres. First, monodisperse silica nanospheres are functionalized with silicate anions in an alkaline solution generated by the hydrolysis of urea. Driven by the interfacial reaction between aqueous solution of nickel nitrate and activated silica nanospheres, uniform deposition of nickel silicate occurs around the scaffold of silica template to form a nickel silicate shell.<sup>28–29</sup> Such  $\text{SiO}_2$ @nickel silicate core-shell structures are readily converted into NiS hollow spheres at an elevated temperature by reacting with sodium sulfide ( $\text{Na}_2\text{S}$ ), where the silica cores are etched simultaneously by  $\text{OH}^-$  released from the hydrolysis of sulfide ions. Herein  $\text{Na}_2\text{S}$  not only serves as sulfurizing agent for the phase transformation from nickel silicate to thermodynamically favored nickel sulfide, but also grants the as-formed hollow spheres structural integrity by providing a mild alkaline environment to gradually remove the silica template. As a result of favorable kinetic control over this process, delicate nanosheets are formed as the subunits of the hierarchical hollow spheres.

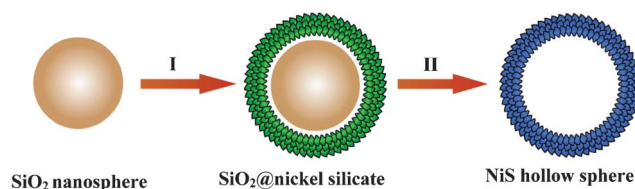


**Fig. 1** Schematic illustration of the formation of NiS hollow spheres by a template-engaged conversion route: (I) uniform precipitation of a nickel silicate shell on silica nanospheres; (II) chemical conversion to NiS hollow spheres with simultaneous template elimination in the presence of  $\text{Na}_2\text{S}$ .

School of Chemical and Biomedical Engineering, Nanyang Technological University, 70 Nanyang Drive, 637457, Singapore.

E-mail: chen0575@ntu.edu.sg; xwlou@ntu.edu.sg

† Electronic supplementary information (ESI) available: More XRD, EDX, BET and TEM data for the nanospheres of  $\text{SiO}_2$ @nickel silicate and NiS. See DOI: 10.1039/c1ra00240f

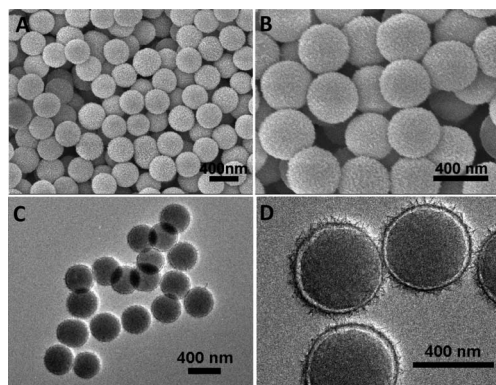


**Fig. 2** (A, B) FESEM images and (C, D) TEM images of core-shell structured  $\text{SiO}_2$ @nickel silicate nanospheres.

The crystallographic phase of  $\text{SiO}_2$ @nickel silicate was investigated by X-ray diffraction (XRD, Fig. S1†). All diffraction peaks can be assigned to the  $\text{Ni}_3\text{Si}_2\text{O}_5(\text{OH})_4$  phase<sup>30</sup> without noticeable signals from possible impurities such as nickel hydroxides. A panoramic view of  $\text{SiO}_2$ @nickel silicate products reveals that the sample consists entirely of uniform nanospheres without impurity particles or aggregates, as depicted in field-emission scanning electron microscopy (FESEM) images (Fig. 2A and B). These nanospheres inherit the original spherical shape of the silica templates with a diameter of around 400 nm, and the uniform coating of nickel silicate on the entire surface of silica nanospheres is evidenced by the void space between the silica core and the shell with a very thin thickness of *ca.* 10 nm, as shown in transmission electron microscopy (TEM) images (Fig. 2C and D).

After simple reaction with  $\text{Na}_2\text{S}$  in solution, uniform NiS hollow spheres assembled from ultrathin nanosheets can be produced without losing the spherical morphology, as shown in Fig. 3A. The complete phase conversion is confirmed by XRD analysis (Fig. 3B), where all the identified peaks can be ascribed to the hexagonal NiS phase (JCPDS No. 12-0041) without nickel silicate residue.<sup>27</sup> The hollow interior and geometrical structure of as-synthesized NiS spheres are further elucidated by TEM examination, as displayed in Fig. 3C and D. In good agreement with the SEM finding, a high uniformity of hollow spheres can be observed from the images, and the inner cavity is clearly revealed by the contrast between NiS shell and hollow interior. No apparent collapse of the shell is observed owing to the good structural stability and integrity of the hollow spheres. Further high-resolution TEM observation evidences the presence of ultrathin nanosheets around the shell, of which the thickness is as thin as only a few nanometres (Fig. 3E and F). Energy dispersive spectra (see ESI, Fig. S2†) indicate the presence of a small amount of Si, that is likely due the amorphous silicate residue.  $\text{N}_2$  adsorption/desorption measurement (see ESI, Fig. S3†) shows that these hollow spheres possess a large Brunauer–Emmett–Teller (BET) specific surface area of *ca.*  $211 \text{ m}^2 \text{ g}^{-1}$  with uniform 4 nm mesopores. Apparently, such a hierarchical hollow structure holds greater promise in offering sufficient surface area to facilitate electrochemical reactions with respect to their bulk or solid counterparts. Furthermore, the use of pre-grown silica templates allows the structural feature of resultant NiS hollow spheres to be rationally controlled in different structural levels. For example, analogous hollow colloids with smaller dimension and interior volume (*e.g.*, 200 nm) can be prepared through the same protocol by templating

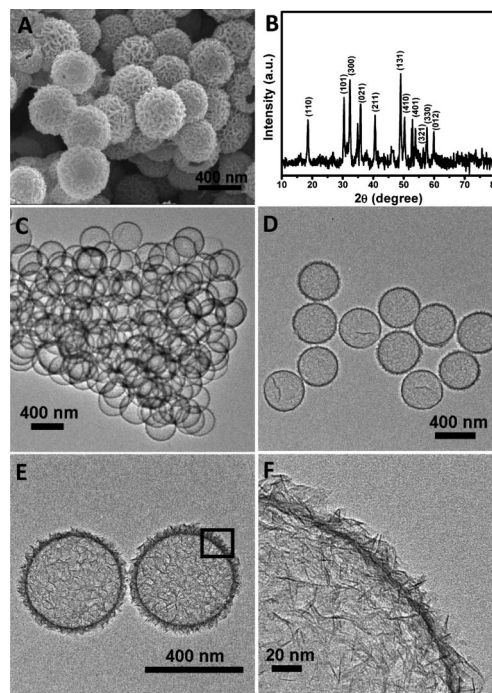


**Fig. 3** (A) FESEM image, (B) XRD pattern and (C–F) TEM images of NiS hierarchical hollow spheres (F is taken from the rectangle area in E).

against silica nanospheres with a corresponding size (see ESI, Fig. S4†). By introducing a co-solvent such as ethanol into the conversion system, the surface texture of these hollow spheres can be further tailored into thicker shells assembled from larger nanosheets with a denser packing (see ESI, Fig. S5†).

With high conductivity at room temperature, NiS is a very appealing candidate as one electrode material for supercapacitors. Generally, its capacitance is mainly derived from the pseudo-capacitive charging and discharging based on the following reversible redox reaction:



In the present work, this reversible reaction gives rise to a pair of redox peaks in the potential range of  $-0.15$ – $0.55 \text{ V}$  by cyclic voltammetry (CV) analysis at various scan rates (Fig. 4A).<sup>31</sup> This CV profile suggests a distinctly different pseudo-capacitive characteristics from normal electric double-layer capacitance with a rectangular CV shape.<sup>32</sup> The anodic peak at about  $0.5 \text{ V}$  from the CV curves is well manifested as a plateau in the galvanostatic charge curves shown in Fig. 4B. The potential plateaus observed in the charge curves correspond to the anodic process. With higher current densities, this plateau will shift to a higher voltage because of stronger polarization. The galvanostatic charge/discharge tests demonstrate high average specific capacitances of  $927 \text{ F g}^{-1}$  and  $618 \text{ F g}^{-1}$  at current densities of  $4.08 \text{ A g}^{-1}$  and  $8.16 \text{ A g}^{-1}$ , respectively (Fig. 4C). At a higher current density of  $10.2 \text{ A g}^{-1}$ , a specific capacitance of  $583 \text{ F g}^{-1}$  can still remain that is around 62.8% of the capacitance at  $4.08 \text{ A g}^{-1}$ . Fig. 4D shows the cycling performance of NiS hollow spheres at a current density of  $4.2 \text{ A g}^{-1}$  in a voltage window of  $-0.15$ – $0.55 \text{ V}$ . At such a relatively high current density, the initial capacitance is  $823 \text{ F g}^{-1}$ , and a capacitance of  $587.1 \text{ F g}^{-1}$  can be retained after 1000 cycles. Such a good electro-capacitive performance may be

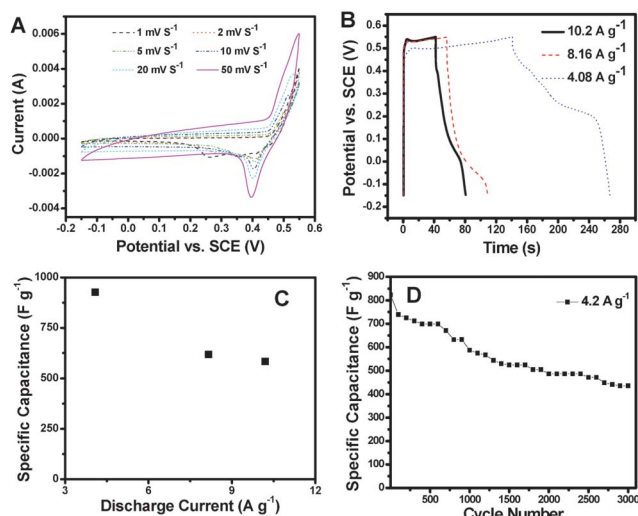


**Fig. 4** (A) CV curves of NiS hollow spheres in the range of  $-0.15$  V– $0.55$  V at various scan rates; (B) galvanostatic charge-discharge curves and (C) average specific capacitance of NiS hollow spheres at various current rates; (D) cycling performance of NiS hollow spheres at a current rate of  $4.2\text{ A g}^{-1}$ .

attributed to the unique structural features of these NiS hollow spheres. Specifically, the very high surface area and hierarchical porous structure composed of ultrathin nanosheets offer a large interfacial area between the electrode material and the electrolyte and sufficient physical cavities for fast ionic diffusion, respectively.<sup>33</sup> After extended cycling for another 2000 cycles, around 74.1% of the capacitance at the 1000th cycle can still be maintained, evidently showing its relatively high cycling stability. This improved capacitance retention may be attributed to the enhanced structural integrity of these hierarchical hollow spheres.<sup>34</sup> Nonetheless, it should be pointed out that after prolonged charge-discharge cycling, some of the NiS hollow spheres will be collapsed because of the ultrathin nanosheet shell structure (see ESI, Fig. S6†), leading to the capacitive decay observed from Fig. 4D.

In summary, we have developed an efficient template-engaged conversion route for the preparation of hierarchical NiS hollow spheres assembled from ultrathin nanosheets under hydrothermal conditions. The as-prepared NiS hollow spheres are shown to be very uniform in size, mesoporous in textural property, and structurally robust benefiting from the *in situ* template removal. In virtue of the unique structural features, these NiS hollow spheres exhibit high specific capacitances of  $583\text{--}927\text{ F g}^{-1}$  at various current densities of  $4.08\text{--}10.2\text{ A g}^{-1}$ . Over 70% of the initial capacitances can be retained even after deep cycling of 1000–3000 cycles. This suggests their promising application as electrode materials for high-performance supercapacitors.

## Experimental

### Synthesis of core-shell structures of $\text{SiO}_2$ @nickel silicate

The  $\text{SiO}_2$ @nickel silicate nanospheres were first prepared by a reported method with slight modification.<sup>30</sup> In a typical synthesis,  $0.2\text{ g}$  of silica nanospheres were dispersed in  $40\text{ ml}$  of de-ionized (DI) water in a capped bottle, followed by addition of  $1\text{ g}$  of urea and  $0.18\text{ g}$  of  $\text{Ni}(\text{NO}_3)_2 \cdot 6\text{H}_2\text{O}$ . The thoroughly mixed solution was stored

in an electric oven at  $105\text{ }^\circ\text{C}$  for  $12\text{ h}$ . After cooling down naturally, the product was harvested by several rinse-centrifugation cycles and was fully dried at  $60\text{ }^\circ\text{C}$  for further use.

### Synthesis of NiS hierarchical hollow spheres

$0.1\text{ g}$  of above synthesized  $\text{SiO}_2$ @nickel silicate nanospheres was dispersed in  $40\text{ ml}$  of DI water in a Teflon container, followed by addition of  $0.1\text{ g}$  of  $\text{Na}_2\text{S}$ . After thorough mixing, the mixture was heated at  $160\text{ }^\circ\text{C}$  for  $12\text{ h}$ . After cooling down naturally, the black precipitates were collected by several rinse-centrifugation cycles before drying at  $60\text{ }^\circ\text{C}$  in vacuum for the characterization.

### Material characterization

All samples were characterized by field-emission scanning electron microscopy (FESEM, JEOL, JSM-6340F), transmission electron microscopy (TEM, JEOL, JEM-2010) and X-ray diffraction (XRD, Bruker, D8-Advance X-ray Diffractometer, Cu K $\alpha$ ). Measurements of specific surface area and porosity were carried out at  $77\text{ K}$  with a Quantachrome NOVA-3000 system.

### Electrochemical measurements

The electrodes were prepared by mixing NiS hollow spheres with carbon black (super-P-Li) and polyvinylidene difluoride (PVDF) at a weight ratio of  $8 : 1 : 1$ . After thorough mixing, the slurry was pressed onto Ni foam and was dried at  $60\text{ }^\circ\text{C}$  in vacuum overnight. The electrochemical tests were conducted with a CHI 660C electrochemical workstation in an aqueous KOH electrolyte ( $2.0\text{ M}$ ) with a three-electrode cell where Pt foil serves as the counter electrode and a standard calomel electrode (SCE) as the reference electrode.

### Acknowledgements

The authors are grateful to the Ministry of Education (Singapore) for financial support through the AcRF Tier-1 grant (RG 63/08, M52120096).

### References

- X. W. Lou, L. A. Archer and Z. C. Yang, *Adv. Mater.*, 2008, **20**, 3987–4019.
- X. W. Lou, C. M. Li and L. A. Archer, *Adv. Mater.*, 2009, **21**, 2536–2539.
- H. Ma, F. Y. Cheng, J. Chen, J. Z. Zhao, C. S. Li, Z. L. Tao and J. Liang, *Adv. Mater.*, 2007, **19**, 4067–4070.
- N. Du, H. Zhang, J. Chen, J. Y. Sun, B. D. Chen and D. R. Yang, *J. Phys. Chem. B*, 2008, **112**, 14836–14842.
- H. P. Liang, H. M. Zhang, J. S. Hu, Y. G. Guo, L. J. Wan and C. L. Bai, *Angew. Chem., Int. Ed.*, 2004, **43**, 1540–1543.
- S. W. Kim, M. Kim, W. Y. Lee and T. Hyeon, *J. Am. Chem. Soc.*, 2002, **124**, 7642–7643.
- B. X. Li, Y. Xie, M. Jing, G. X. Rong, Y. C. Tang and G. Z. Zhang, *Langmuir*, 2006, **22**, 9380–9385.
- J. H. Lee, *Sens. Actuators, B*, 2009, **140**, 319–336.
- H. R. Kim, K. I. Choi, K. M. Kim, I. D. Kim, G. Z. Cao and J. H. Lee, *Chem. Commun.*, 2010, **46**, 5061–5063.
- J. F. Chen, H. M. Ding, J. X. Wang and L. Shao, *Biomaterials*, 2004, **25**, 723–727.
- Y. F. Zhu, J. L. Shi, W. H. Shen, X. P. Dong, J. W. Feng, M. L. Ruan and Y. S. Li, *Angew. Chem., Int. Ed.*, 2005, **44**, 5083–5087.
- K. An and T. Hyeon, *Nano Today*, 2009, **4**, 359–373.
- J. Liu, S. Z. Qiao, S. B. Hartono and G. Q. Lu, *Angew. Chem., Int. Ed.*, 2010, **49**, 4981–4985.



- 14 J. Liu, S. B. Hartono, Y. G. Jin, Z. Li, G. Q. Lu and S. Z. Qiao, *J. Mater. Chem.*, 2010, **20**, 4595–4601.
- 15 L. Zhang, S. Z. Qiao, Y. G. Jin, Z. G. Chen, H. C. Gu and G. Q. Lu, *Adv. Mater.*, 2008, **20**, 805–809.
- 16 Z. Z. Yang, Z. W. Niu, Y. F. Lu, Z. B. Hu and C. C. Han, *Angew. Chem., Int. Ed.*, 2003, **42**, 1943–1945.
- 17 F. Caruso, R. A. Caruso and H. Mohwald, *Science*, 1998, **282**, 1111–1114.
- 18 X. M. Sun and Y. D. Li, *Angew. Chem., Int. Ed.*, 2004, **43**, 597–601.
- 19 C. H. Lai, K. W. Huang, J. H. Cheng, C. Y. Lee, W. F. Lee, C. T. Huang, B. J. Hwang and L. J. Chen, *J. Mater. Chem.*, 2009, **19**, 7277–7283.
- 20 X. J. Zhu, Z. Y. Wen, Z. H. Gu and S. H. Huang, *J. Electrochem. Soc.*, 2006, **153**, A504–A507.
- 21 T. Takeuchi, H. Sakaabe, H. Kageyama, T. Sakai and K. Tatsumi, *J. Electrochem. Soc.*, 2008, **155**, A679–A684.
- 22 J. Wang, S. Y. Chew, D. Wexler, G. X. Wang, S. H. Ng, S. Zhong and H. K. Liu, *Electrochem. Commun.*, 2007, **9**, 1877–1880.
- 23 K. Aso, H. Kitaura, A. Hayashi and M. Tatsumisago, *J. Mater. Chem.*, 2011, **21**, 2987–2990.
- 24 W. Zhou, W. M. Chen, J. W. Nai, P. G. Yin, C. P. Chen and L. Guo, *Adv. Funct. Mater.*, 2010, **20**, 3678–3683.
- 25 P. T. Zhao, Q. M. Zeng and K. X. Huang, *Mater. Lett.*, 2009, **63**, 313.
- 26 Y. Hu, J. F. Chen, W. M. Chen, X. H. Lin and X. L. Li, *Adv. Mater.*, 2003, **15**, 726–729.
- 27 X. C. Jiang, Y. Xie, J. Lu, L. Y. Zhu, W. He and Y. T. Qian, *Adv. Mater.*, 2001, **13**, 1278–1281.
- 28 Y. Q. Wang, C. J. Tang, Q. A. Deng, C. H. Liang, D. H. L. Ng, F. L. Kwong, H. Q. Wang, W. P. Cai, L. D. Zhang and G. Z. Wang, *Langmuir*, 2010, **26**, 14830–14834.
- 29 J. Zheng, B. H. Wu, Z. Y. Jiang, Q. Kuang, X. L. Fang, Z. X. Xie, R. B. Huang and L. S. Zheng, *Chem.–Asian J.*, 2010, **5**, 1439–1444.
- 30 P. Jin, Q. W. Chen, L. Q. Hao, R. F. Tian, L. X. Zhang and L. Wang, *J. Phys. Chem. B*, 2004, **108**, 6311–6314.
- 31 H. L. Wang, H. S. Casalongue, Y. Y. Liang and H. J. Dai, *J. Am. Chem. Soc.*, 2010, **132**, 7472–7477.
- 32 H. Pang, Q. Y. Lu, Y. C. Lia and F. Gao, *Chem. Commun.*, 2009, 7542–7544.
- 33 M. Q. Wu, G. A. Snook, G. Z. Chen and D. J. Fray, *Electrochem. Commun.*, 2004, **6**, 499–504.
- 34 T. Zhu, J. S. Chen and X. W. Lou, *J. Mater. Chem.*, 2010, **20**, 7015–7020.